

# Neutron DVCS Measurements with BONuS12 in CLAS12

M. Hattawy<sup>‡</sup>, M. Amaryan, S. Bültmann, G. Dodge, N. Dzubenski, C. Hyde, S. Kuhn<sup>†</sup>,  
D. Payette, J. Poudel, L. Weinstein  
*Old Dominion University, Norfolk, VA 23529, USA*

R. Dupré<sup>†</sup>, M. Guidal, D. Marchand, C. Muñoz, S. Niccolai, E. Voutier  
*Institut de Physique Nucléaire, CNRS-IN2P3, Univ. Paris-Sud, Université Paris-Saclay,  
91406 Orsay Cedex, France*

K. Hafidi  
*Argonne National Laboratory, Lemont, IL 60439, USA*

L. El-Fassi  
*Mississippi State University, Mississippi State, MS 39762, USA*

N. Baltzell, G. Gavalian, F. X. Girod, S. Stepanyan  
*Thomas Jefferson National Accelerator Facility, Newport News, VA 23606, USA*

I. Albayrak, E. Christy, A. Nadeeshani  
*Hampton University, Hampton, VA 23669, USA*

N. Kalantarians  
*Virginia Union University, 1500 N. Lombardy St., Richmond, VA 23220, USA*

## a CLAS Run-Group Addition Proposal

---

<sup>‡</sup>Contact person

<sup>†</sup>Spokesperson

## Abstract

The three-dimensional picture of quarks and gluons in the nucleon is set to be revealed through deeply virtual Compton scattering (DVCS). With the absence of a free neutron target, the deuterium target represents the simplest nucleus to be used to probe the internal 3D partonic structure of the neutron. We propose here to measure the beam spin asymmetry (BSA) in incoherent neutron DVCS together with the approved E-12-06-113 experiment (BONUS12) within the run group F, using the same beam time, simply with addition of beam polarization. The DVCS BSA on the quasi-free neutron will be measured in a wide range of kinematics by tagging the scattered electron and the real photon final state with the spectator proton. We will also measure BSA with all final state particles detected including the struck neutron. The proposed measurements is complementary to the approved CLAS12 experiment E12-11-003, which will also measure the quasi-free neutron DVCS by detecting the scattered neutron, but not the spectator proton. Indeed, besides providing more data for neutron DVCS, it would allow comparing the measurements of BSA of neutron DVCS, from the approved measurement E12-11-003 and with the two methods proposed herein. This comparison will help to understand the impact of nuclear effects, such as the final state interactions (FSI) and Fermi motion on the measurement of the neutron DVCS.

# Contents

<b>Abstract</b>	<b>5</b>
<b>Introduction</b>	<b>7</b>
<b>1 Neutron Partonic Structure</b>	<b>8</b>
1.1 Physics motivations: Neutron GPDs . . . . .	8
1.2 DVCS Formalism and Observables . . . . .	9
1.3 Measuring the neutron DVCS . . . . .	11
1.3.1 Two new methods for two objectives . . . . .	11
1.3.2 Tagged neutron DVCS with BONuS12 . . . . .	12
1.3.3 Fully exclusive neutron DVCS with BONuS12 . . . . .	14
<b>2 Run conditions and Experimental setup</b>	<b>15</b>
2.1 Run Group F conditions . . . . .	15
2.2 The CLAS12 Spectrometer . . . . .	15
2.3 BONuS12 RTPC . . . . .	16
2.4 Beam Polarization . . . . .	19
<b>3 Projections for the Proposed Measurements</b>	<b>20</b>
3.1 Monte-Carlo Simulation . . . . .	20
3.2 Particle Identification . . . . .	21
3.2.1 Electron Identification . . . . .	21
3.2.2 Proton Identification . . . . .	21
3.2.3 Neutrals Identification . . . . .	22
3.3 Beam-Spin Asymmetry . . . . .	24
3.4 Projections . . . . .	25
3.4.1 Tagged n-DVCS Projections . . . . .	25
3.4.2 Fully exclusive n-DVCS projections . . . . .	26
<b>4 Additional Physics Measurements with Run Group F</b>	<b>32</b>
<b>Summary</b>	<b>33</b>

# Introduction

Inclusive deep inelastic scattering (DIS) experiments have been instrumental in advancing our understanding of the QCD structure of nucleons in the past. More recently, hard exclusive experiments such as Deeply Virtual Compton Scattering (DVCS) and Deeply Virtual Meson Production (DVMP) have provided important new probes that allow us to explore both the motion of partons and their transverse spatial structure in nucleons through the generalized parton distribution (GPD) framework. The GPDs correspond to the coherence between quantum states of different (or same) helicity, longitudinal momentum, and transverse position. In an impact parameter space, they can be interpreted as a distribution in the transverse plane of partons carrying a certain longitudinal momentum [1–3]. A crucial feature of GPDs is the access to the transverse position of partons which, combined with their longitudinal momentum, leads to the total angular momentum of partons [4]. This information is not accessible to inclusive DIS which measures probability amplitudes in the longitudinal plane.

A high luminosity facility such as Jefferson Lab offers a unique opportunity to map out the three-dimensional quark and gluon structure of nucleons and nuclei. While most of submitted proposals to JLab Program Advisory Committee (PAC) have focused on the studies of the 3D proton structure considered as one of the main motivations for the JLab 12 GeV upgrade, we propose here to extend the measurements to quasi-free neutrons in deuterium with BONuS12 experiment. Such measurement is critical in the Jefferson Lab GPD program for two aspects, first as neutrons offer the only access to flavor decomposition for GPDs, second because of the importance of the  $E$  GPD to measure the Ji sum rule [5, 6].

Recent results from CLAS on incoherent DVCS from a  $^4\text{He}$  target have shown that even in light nuclei, large nuclear effects can be observed [7]. As this measurement shows a deviation of  $\approx 30\%$  for the beam spin asymmetry (BSA) of DVCS of bound proton in helium, one can assume that a sizable correction will be necessary in the neutron case as well. This could be particularly dramatic as the BSA expected on neutrons are rather small. We propose here to transpose the methods developed for BONuS12 for PDF measurements [8] to the GPDs. In particular, we are looking how the initial state and the break-up of the deuterium might affect measured BSA. The run group F is the perfect occasion to gather data on this topic, which can be done with the simple addition of beam polarization to the setting of the run group!

# Chapter 1

## Neutron Partonic Structure

### 1.1 Physics motivations: Neutron GPDs

A wealth of information on the structure of hadrons lies in the correlations between the momentum and spatial degrees of freedom of the partons. These correlations can be revealed through deeply virtual Compton scattering (DVCS), i.e., the hard exclusive lepto-production of a real photon, which provides access to a three-dimensional (3-D) imaging of partons within the generalized parton distributions (GPDs) framework [5, 9–12]. The measurement of free proton DVCS has been the focus of a worldwide effort [13–21] involving several accelerator facilities such as Jefferson Lab, DESY and CERN. These measurements now enable the extractions of GPDs and a 3-D tomography of the free proton [22, 23]. The aim of this proposal is enhance the neutron GPD measurements along the approved CLAS12 experiment E12-11-003, which will also measure the quasi-free neutron DVCS by detecting the scattered neutron in deuterium.

In the fits of PDFs, [24] for example, neutrino and deuterium data allow to make a flavor dependent extraction, this option is not available for GPDs yet due to the lack of reliable data. Indeed, the observables of DVCS, such as cross sections and beam-spin asymmetries are much smaller on neutron targets, while the nuclear effects in deuterium increase uncertainties. These issues have lead to results [25] which are not precise enough to help in a flavor dependent GPD extraction. To achieve this performance, one will need a large quantity of high precision data a goal set by the E-12-11-003. However, the impact of the uncertain initial state and the final state interactions on the integration of these data in global fits remain unclear. With this proposal, we propose to both provide more data on the neutron, which is always important, but most importantly these data will have completely independent systematic errors from the E-12-11-003 data. That will make them complementary and indicate in what ways these methods are equivalent or potentially need *ad hoc* corrections.

Neutron DVCS is also hoped to provide an important contribution to the extraction of the GPD  $E$  [26]. The reasoning behind this expectation is as follows, the GPD  $E$  never appears to be dominant in usually measured DVCS observables, as a sub-leading contribution it is

always plagued with large error bars. Actually, recent extractions [27, 28] show that we still barely have any constraint on  $E$  using all the world proton data. However, as form factors often appear in the expressions of DVCS observables because of the Bethe Heitler process (see below) the situation is very different for protons and neutrons. Indeed, the  $F_1$  form factor of the neutron is very small, making the  $E$  GPD more prominent in some of the neutron DVCS observables. Most notably the sin component of the beam spin asymmetry (see Eq. 1.9 below for details) is given by [26]:

$$s_{1,\text{unp}}^I \propto \Im m \left[ F_1 \mathcal{H} + \xi(F_1 + F_2) \tilde{\mathcal{H}} - \frac{t}{4M^2} F_2 \mathcal{E} \right], \quad (1.1)$$

highlighting the effect of a suppressed  $F_1$  on the main term. This lead to the idea that neutron DVCS will also help significantly to constrain the GPD  $E$ . This goal is of course driven by the long standing objective of GPD physics to measure the Ji sum rule in the nucleon:

$$J_q = \frac{1}{2} \int_{-1}^{+1} dx x [H^q(x, \xi, t=0) + E^q(x, \xi, t=0)], \quad (1.2)$$

which links the total angular momentum ( $J_q$ ) carried by each quark  $q$  to the sum of the second moments over  $x$  of the GPDs  $H$  and  $E$ , that will complete the decomposition of the nucleon spin in its various components [5, 6].

## 1.2 DVCS Formalism and Observables

The cross section for DVCS on a spin-1/2 target can be parameterized in terms of four helicity conserving GPDs:  $H^q$ ,  $E^q$ ,  $\tilde{H}^q$ , and  $\tilde{E}^q$ . The GPDs  $H$ ,  $E$ ,  $\tilde{H}$  and  $\tilde{E}$  are defined for each quark flavor ( $q = u, d, s, \dots$ ). Analogous GPDs exist for the gluons, see references [12, 29] for further details. In this work, we are mostly concerned by the valence quark region, in which the sea quarks and the gluons contributions do not dominate the DVCS scattering amplitude. The GPDs  $H$  and  $\tilde{H}$  conserve the spin of the nucleon, while  $E$  and  $\tilde{E}$  flip it [30]. The  $H$  and  $E$  GPDs are called the unpolarized GPDs as they represent the sum over the different configurations of the quarks' helicities, whereas  $\tilde{H}$  and  $\tilde{E}$  are called the polarized GPDs because they are made up of the difference between the orientations of the quarks' helicities.

The differential cross section of leptonproduction of photons for a longitudinally-polarized electron beam and an unpolarized nucleon target can be written as:

$$\frac{d\sigma}{dx_B dy dt d\phi d\varphi} = \frac{\alpha^3 x_B y}{16\pi^2 Q^2 \sqrt{1 + \varepsilon^2}} \left| \frac{\mathcal{T}}{e^3} \right|^2 \quad (1.3)$$

where  $\varepsilon \equiv 2x_B \frac{M_n}{Q}$ ,  $x_B = Q^2/(2p_1 \cdot q_1)$  is the Bjorken variable,  $y = (p_1 \cdot q_1)/(p_1 \cdot k_1)$  is the photon energy fraction,  $\phi$  is the angle between the leptonic and hadronic planes,  $\varphi$  is the scattered electron's azimuthal angle,  $Q^2 = -q_1^2$ , and  $q_1 = k_1 - k_2$ . The particle momentum

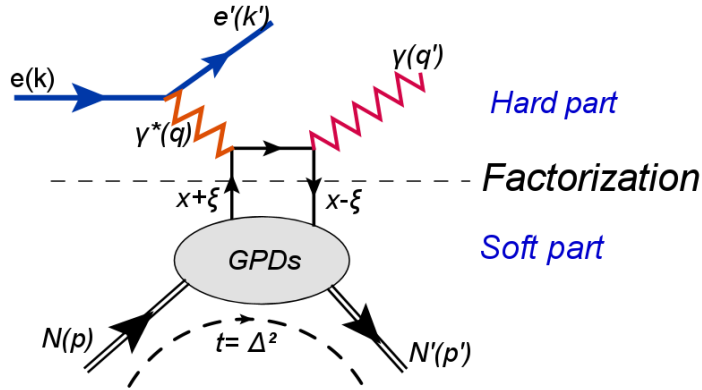


Figure 1.1: Leading-twist DVCS handbag diagram with the momentum definitions labeled.

definitions are shown in Figure 1.1. The momentum transfer where the nucleon is initially at rest,  $\Delta = p_1 - p_2$  and  $t = \Delta^2$ . The Bjorken variable is related to another scaling variable called skewedness:

$$\xi = \frac{x_B}{2 - x_B} + \mathcal{O}(1/Q^2). \quad (1.4)$$

The amplitude is the sum of the DVCS, the Bethe-Heitler (BH), and the interference amplitudes, and when squared has terms

$$\mathcal{T}^2 = |\mathcal{T}_{\text{BH}}|^2 + |\mathcal{T}_{\text{DVCS}}|^2 + \mathcal{I} \quad (1.5)$$

where the first is the BH contribution, the second is the DVCS part, and the last term is the interference part,

$$\mathcal{I} = \mathcal{T}_{\text{DVCS}} \mathcal{T}_{\text{BH}}^* + \mathcal{T}_{\text{DVCS}}^* \mathcal{T}_{\text{BH}}. \quad (1.6)$$

The corresponding amplitudes are calculated with the diagrams shown in Figures 1.1 and 1.2. The details of contracting the DVCS tensor with various currents and tensors can be found in [31]. The resulting expressions for the amplitudes are

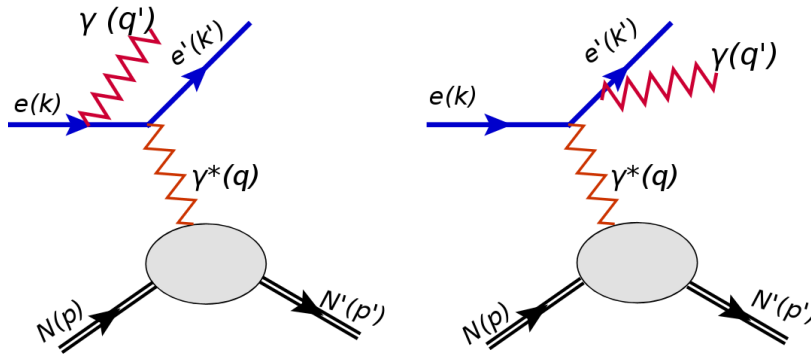


Figure 1.2: BH handbag diagrams.

$$|\mathcal{T}_{\text{BH}}|^2 = \frac{e^6(1 + \varepsilon^2)^{-2}}{x_B^2 y^2 t \mathcal{P}_1(\phi) \mathcal{P}_2(\phi)} \left\{ c_0^{\text{BH}} + \sum_{n=1}^2 [c_n^{\text{BH}} \cos(n\phi) + s_n^{\text{BH}} \sin(n\phi)] \right\} \quad (1.7)$$

$$|\mathcal{T}_{\text{DVCS}}|^2 = \frac{e^6}{y^2 Q^2} \left\{ c_0^{\text{DVCS}} + \sum_{n=1}^2 [c_n^{\text{DVCS}} \cos(n\phi) + s_n^{\text{DVCS}} \sin(n\phi)] \right\} \quad (1.8)$$

$$\mathcal{I} = \frac{e^6(1 + \varepsilon^2)^{-2}}{x_B y^3 t \mathcal{P}_1(\phi) \mathcal{P}_2(\phi)} \left\{ c_0^{\mathcal{I}} + \sum_{n=1}^3 [c_n^{\mathcal{I}} \cos(n\phi) + s_n^{\mathcal{I}} \sin(n\phi)] \right\} \quad (1.9)$$

The functions  $c_0$ ,  $c_n$ , and  $s_n$  are called *Fourier coefficients* and they depend on the kinematic variables and the operator decomposition of the DVCS tensor for a target with a given spin. At leading twist there is a straightforward form factor decomposition which relates the vector and axial-vector operators with the so-called Compton form factors (CFFs) [32]. The Compton form factors appearing in the DVCS amplitudes are integrals of the type

$$\mathcal{F} = \int_{-1}^1 dx F(\mp x, \xi, t) C^\pm(x, \xi) \quad (1.10)$$

where the coefficient functions at leading order take the form

$$C^\pm(x, \xi) = \frac{1}{x - \xi + i\varepsilon} \pm \frac{1}{x + \xi - i\varepsilon}. \quad (1.11)$$

We plan on measuring the beam spin asymmetry as a function of  $\phi$

$$A_{LU}(\phi) = \frac{d\sigma^\uparrow(\phi) - d\sigma^\downarrow(\phi)}{d\sigma^\uparrow(\phi) + d\sigma^\downarrow(\phi)} \quad (1.12)$$

where the arrows indicate the electron beam helicity.

## 1.3 Measuring the neutron DVCS

### 1.3.1 Two new methods for two objectives

As shown in Fig. 1.3, one can measure all the components of the DVCS reaction on deuterium using CLAS and Bonus12. This method, while perfect on the paper, leads to an efficiency problem as both the measurement of the spectator proton and of the neutrons are challenging and low efficiency (intrinsically for the neutron and by the limitation of phase space available for the proton). However, it is possible to ensure the exclusivity of a process when missing one of the final state particles by applying cuts on missing mass, momentum and energy. This strategy can be used, either to leave the spectator proton or the neutron undetected. The former, being used in the ongoing E-12-11-003. We propose here to perform the other option, detecting the spectator proton but not the neutron, in order to increase the amount of available data, but most importantly, to confirm the equivalency of both methods.

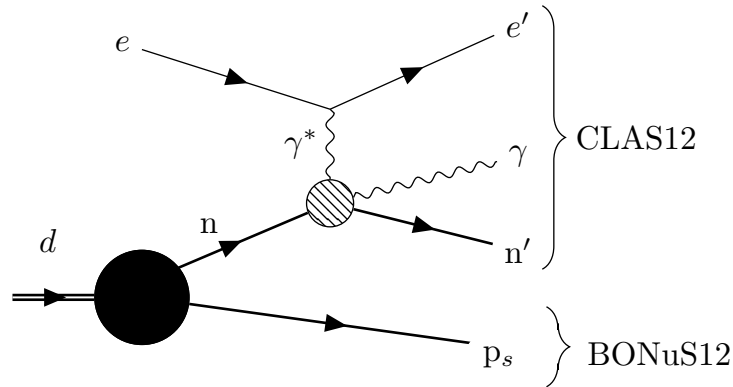


Figure 1.3: Fully exclusive neutron DVCS diagram in deuterium.

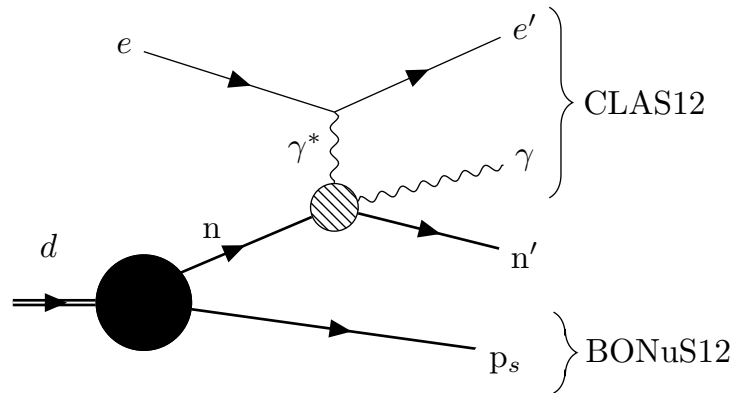


Figure 1.4: Neutron Tagged-DVCS diagram in deuterium.

Moreover, we will be able to perform the fully exclusive measurement, but with rather limited statistics. We intend to use this over-constrained last measurement to study the systematic effects linked to the nuclear target and the uncertainties in detection.

### 1.3.2 Tagged neutron DVCS with BONuS12

The tagged neutron detection scheme is described in Fig. 1.4, where we see that a detector for low energy proton spectators is necessary. Here, we propose to use the Bonus radial TPC, which is designed to make a similar type of measurement for inclusive deeply inelastic scattering. The first goal of the present proposed experiment is simply to provide more data in the field of neutron GPD. Indeed, the measurement of neutron DVCS is very challenging and very little published data is available at this point.

Second, we observe that the systematics from this measurement are going to be mostly independent of the ones from E-12-11-003. Indeed, while this measurement will be missing one of the high energy product of the reaction leading to more uncertainty in exclusivity cuts, it will detect the spectator proton, significantly help with nuclear effects. This has interestingly

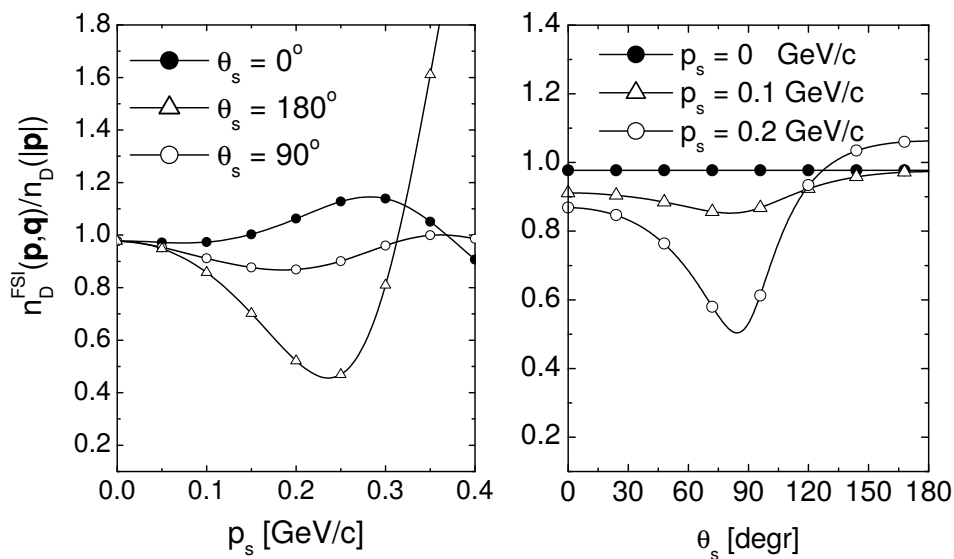


Figure 1.5: Ratio of cross sections for the FSI model from [33] to PWIA calculation as a function of the spectator momentum (left) and spectator angle (right).

an impact on both initial state and final state effects. In the initial state, the neutron is in fact not at rest and carries some Fermi momentum, which can be directly inferred from the kinematic of the spectator proton, thanks to the simple two body deuterium. On the final state side, detecting the spectator proton in a certain range of momentum and angle allows to significantly reduce the probability of final state interactions to have occurred.

In order to resolve the initial state issue, we evaluate the standard Lorentz invariant  $x$  in terms of the spectator kinematics.  $x$  acquires a star to indicate true invariants rather than the values calculated assuming a stationary, on-shell target:

$$x^* = \frac{Q^2}{2M_N E \gamma (2 - \alpha_s)} = \frac{x_B}{2 - \alpha_s}, \quad (1.13)$$

where  $\alpha_s = \frac{E_s - p_s^z}{M_N}$ , with  $M_N$ ,  $E_s$ , and  $p_s^z$  are the on-shell mass, energy, and z-momentum component of the spectator proton.

To understand the regions where final state interactions are expected to be significant, we look at the spectator momentum and angle relative to the momentum transfer,  $\theta_s$ . In Figure 1.5 [33, 34], we see calculations for the inclusive case. At low recoil momentum and backwards spectator angle, the FSIs are negligible, where at high momenta perpendicular to the momentum transfer, the FSIs are maximized.

It is important to note that the detection of the neutron or the spectator proton are not equivalent. While it could appear to be so after applying the exclusivity cut, it is not the case because of the large uncertainty (a percent or more) in the energy measurement of photons. This uncertainty is larger than the momentum of the spectator proton and therefore completely hinders our capability to reconstruct it, if it is not directly measured.

---

In conclusion, the measurement of this channel will offer a similar amount of data as other CLAS12 measurements but with different systematic effects. In particular, reducing the impact of the least known nuclear effects.

### 1.3.3 Fully exclusive neutron DVCS with BONuS12

As highlighted above, the fully exclusive measurement of neutron DVCS is plagued by two difficult particles to measure, a slow proton and a fast neutron. However, it can still provide relevant information in a limited kinematic space. As this measurement is fully exclusive, it provides over-constraints by using missing mass, momentum and energy cuts. This will give us a particularly clean sample of data with a minimal amount of corrections to be applied and the best control over systematic errors. We propose to use this sample, that can only be obtained using a recoil detector, to study the effects described above of Fermi motion, final state interactions and incomplete detection of the final state. This will confirm assumptions made in other neutron DVCS measurements and help understand better their systematic errors.

# Chapter 2

## Run conditions and Experimental setup

### 2.1 Run Group F conditions

Run Group F (E12-06-113) has been approved to collect 35 PAC days (100% efficiency) of data on deuterium with 10.7 GeV electron beam and another six days on hydrogen. One of the days of hydrogen data taking will be carried out with a low energy electron beam of about 2.2 GeV. The 40 cm long target filled with 7 atm deuterium gas at room temperature and the 200 nA electron beam will yield a combined luminosity of about  $2 \times 10^{34} \text{cm}^{-2} \text{s}^{-1}$ , about a factor of five below the standard CLAS12 luminosity.

For the detection of the recoil protons, Run Group F is going to install a new and enlarged radial time projection chamber (RTPC) and target gas cell assembly, very similar to the ones used by the BoNuS (E03-012) and eg6 (E08-024) experiments. The RTPC can detect proton recoil momenta down to a lower limit of 70 MeV/c while being insensitive to minimum ionizing particles. The RTPC will be replacing the central detector's silicon tracker and barrel micromegas, while keeping an updated design of the forward micromegas (FMT). In the updated design of the FMT, only three layers of micromegas will be kept to improve the electron's reconstructed vertex resolution while reducing the material in the path of the electrons. In the following sections we briefly introduce the experimental setup of Run Group F.

### 2.2 The CLAS12 Spectrometer

The CLAS12 spectrometer is designed to operate with 11 GeV beam at an electron-nucleon luminosity of  $\mathcal{L} = 1 \times 10^{35} \text{cm}^{-2} \text{s}^{-1}$ . The baseline configuration of the CLAS12 detector consists of the forward detector and the central detector packages [35] (see Figure 2.1). The CLAS12 Central Detector [35] is designed to detect various charged particles

over a wide momentum and angular range. The main detector package includes:

- Solenoid Magnet: provides a central longitudinal magnetic field up to 5 Tesla, which serves to curl emitted low energy Møller electrons and determine particle momenta through tracking in the central detector.
- Central Tracker: consists of 3 double layers of silicon strips and 6 layers of Micromegas. The thickness of a single silicon layer is 320  $\mu\text{m}$ .
- Central Time-of-Flight: an array of scintillator paddles with a cylindrical geometry of radius 26 cm and length 50 cm; the thickness of the detector is 2 cm with designed timing resolution of  $\sigma_t = 50$  ps, used to separate pions and protons up to 1.2 GeV/c.

We will use the forward detector for electron, photon, and neutron detection. The central detector's silicon tracker and barrel micromegas will be removed to leave room for the BONuS12 RTPC for the detection of the slow recoiling protons in deuterium. In addition to the main sub-detectors of CLAS12 Central detector, we will be using the Central Neutron Detector (CND) for the detection of the final state recoiling neutrons.

The scattered electron, photon, and neutron will be detected in the forward detector which consists of the High Threshold Cherenkov Counters (HTCC), Drift Chambers (DC), the Low Threshold Cherenkov Counters (LTCC), the Time-of-Flight scintillators (TOF), the Forward Calorimeter and the Preshower Calorimeter. The charged particle identification in the forward detector is achieved by utilizing the combination of the HTCC, LTCC and TOF arrays with the tracking information from the Drift Chambers. The HTCC together with the Forward Calorimeter and the Preshower Calorimeter will provide a pion rejection factor of more than 2000 up to a momentum of 4.9 GeV/c, and a rejection factor of 100 above 4.9 GeV/c. The photons and the neutrons are detected using the calorimeters. As will be showing later on, the majority of the final state recoiling neutrons will be detected using the sub-detectors of CLAS12 Central Detector, in particular CTOF and CND.

## 2.3 BONuS12 RTPC

The new CLAS12 RTPC (BONuS12) is an active 400 mm long cylinder of 160 mm diameter, leaving just enough room to fit adaptive readout boards between the RTPC outer shell and the CTOF. The electric field is directed perpendicularly to the beam direction, such that drifting electrons are pushed away from the beam line. These electrons are amplified by three layers of cylindrical gas electron multipliers (GEM) and detected by the readout system on the external shell of the detector as illustrated in Figure 2.2. The BONuS12 RTPC covers almost 100% of the azimuthal angle range.

We detail here the different regions shown in Figure 2.2 starting from the beam line towards larger radius:

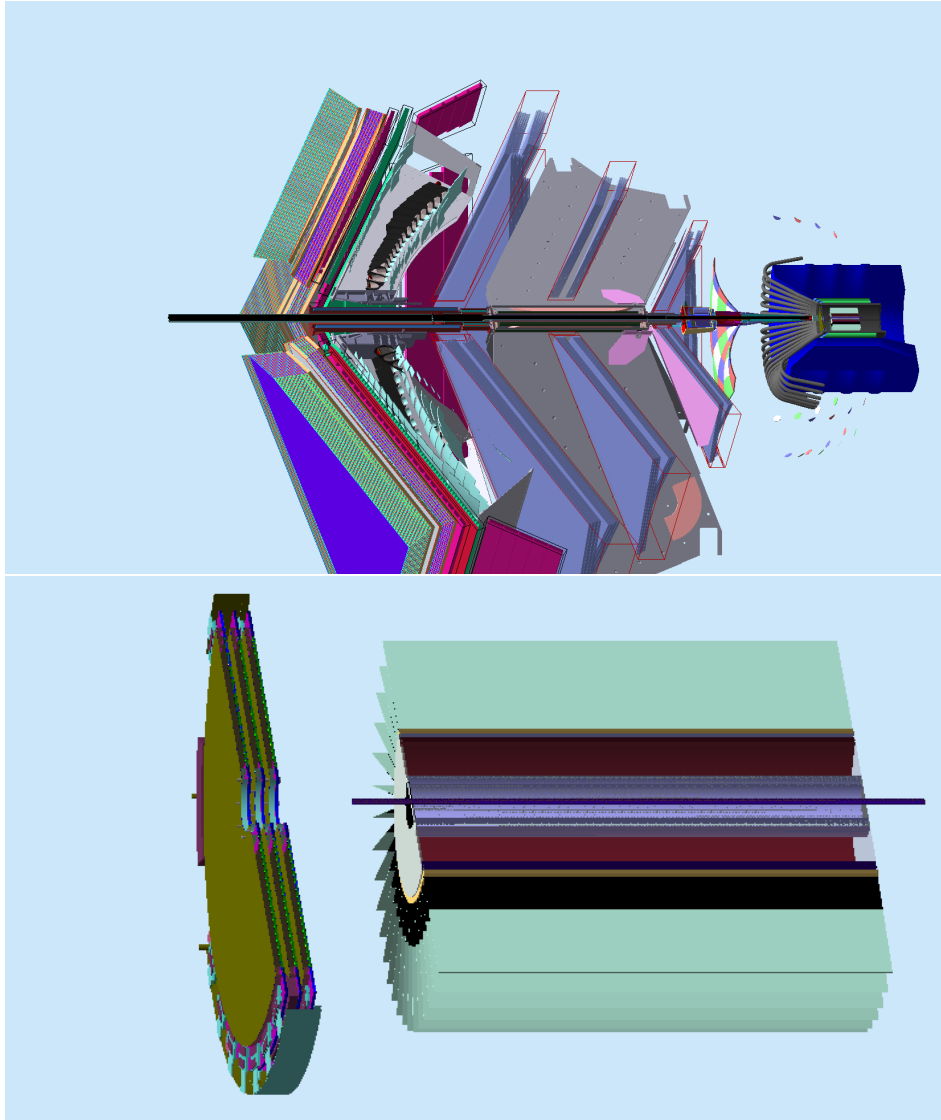


Figure 2.1: (Top) The schematic layout of the CLAS12 baseline design with BONuS12 RTPC replacing the silicon tracker and the barrel micromegas. (Bottom) Schematic layout showing BONuS12 RTPC with the modified design of the forward micromegas.

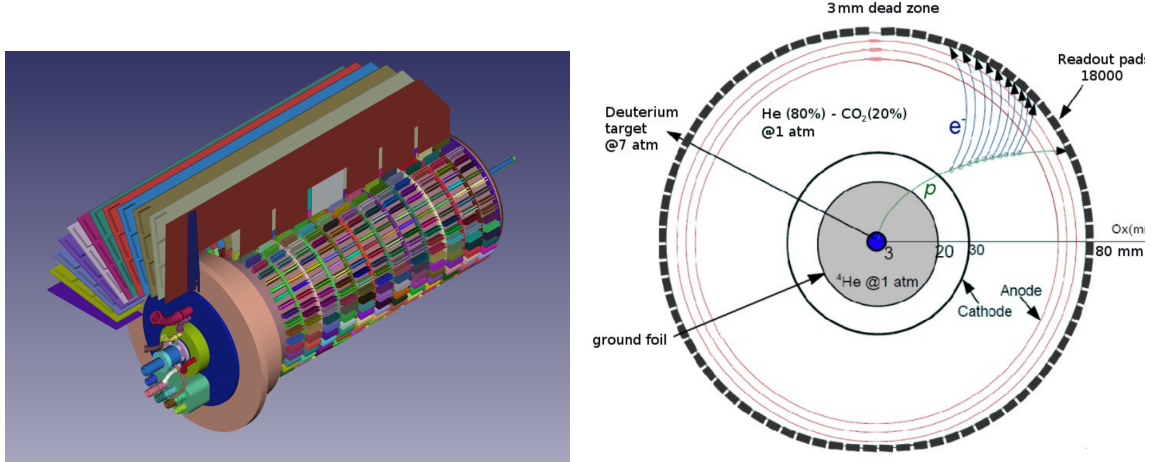


Figure 2.2: (Left) Schematic layout showing BONuS12 RTPC showing the readout padboard and few adaptive boards in addition to the gas lines. (Right) Schematic drawing of the CLAS RTPC in a plane perpendicular to the beam direction. See text for description of the elements.

- The 7 atm Deuterium gas target extends along the beamline forming the detector central axis. It is a 6 mm diameter Kapton straw with a  $50 \mu\text{m}$  wall of 492 mm length such that its entrance and exit  $15 \mu\text{m}$  aluminum windows are placed outside of the detector volume. The detector and the target are placed in the center of the solenoid, 64 cm upstream of the CLAS12 center.
- The first gas gap covers the radial range from 3 mm to 20 mm. It is filled with  $^4\text{He}$  gas at 1 atm to minimize secondary interactions from Møller electrons scattered by the beam. This region is surrounded by a  $4 \mu\text{m}$  thick window made of grounded aluminized Mylar.
- The second gas gap region extends between 20 mm and 30 mm and is filled with the gas mixture of 80%  $^4\text{He}$  and 20%  $\text{CO}_2$ . This region is surrounded by a  $4 \mu\text{m}$  thick window made of aluminized Mylar set at  $-4260 \text{ V}$  to serve as the cathode.
- The drift region is filled with the same  $^4\text{He}\text{-CO}_2$  gas mixture and extends from the cathode to the first GEM, 70 mm away from the beam axis. The electric field in this region is perpendicular to the beam and averages around  $550 \text{ V/cm}$ .
- The electron amplification system is composed of three GEMs located at radii of 70, 73 and 76 mm. The first GEM layer is set to  $\Delta V = 1620 \text{ V}$  relative to the cathode foil and then each subsequent layer is set to a lower voltage relative to the previous to obtain a strong ( $\sim 1600 \text{ V/cm}$ ) electric field between the GEM foils. A 275 V bias is applied across each GEM for amplification.

- The readout board has an internal radius of 79 mm and collects charges after they have been multiplied by the GEMs. Adaptive readout circuit boards are plugged directly on its outer side and transmit the signal to the data acquisition electronics.

## 2.4 Beam Polarization

For our proposed measurements we ask for the electron beam to be highly polarized, i.e., 85% longitudinally polarized beam, which is the average achieved polarization of the beam during Run Group A and Run Group B using the upgraded 12 GeV experimental setup. Regarding measuring the beam polarization, no additional commissioning time is required. The spokespersons of Run Group F [36] has accepted to provide commissioning time to perform Møller run once a week, which is enough for the proposed measurements.

# Chapter 3

## Projections for the Proposed Measurements

In this work we propose to measure the neutron's DVCS beam-spin asymmetry in the following two channels:

1. Tagged n-DVCS:  $D + \gamma^* \longrightarrow \gamma + (n) + p$
2. Fully exclusive n-DVCS:  $D + \gamma^* \longrightarrow \gamma + n + p$

To demonstrate the experimental feasibility and to extract projections for our proposed measurements, we present here a simulation study using a realistic n-DVCS event generator and the official simulation-reconstruction chain of CLAS12 spectrometer upgraded with BONuS12 RTPC.

### 3.1 Monte-Carlo Simulation

An event generator for DVCS/BH and exclusive  $\pi^0$  electroproduction on the neutron inside a deuterium target has been developed [37]. The DVCS amplitude is calculated according to the BKM formalism [31], while the GPDs have been taken from the VGG model [38, 39]. The Fermi-motion distribution is calculated with the Paris potential [40].

The output of the event generator was fed through CLAS12 official simulation (GEMC 4.3.0) [41] and reconstruction (COATJAVA 5b.7.4) [42] chain, to simulate the detectors' acceptance and resolutions for the following final state particles, electrons, photons, and neutrons, within the proposed experimental setup of Run Group F. Spectator protons are reconstructed with a fastMC that was developed based on the performance of the eg6 CLAS run.

## 3.2 Particle Identification

The final state of neutron Tagged-DVCS event consists of three particles: an electron, a proton, and a real photon, while in addition to these particles a neutron is required to be detected in the fully exclusive neutron's DVCS events. To identify the DVCS events, we first identify the different particles of interest. Then, events with three and four detected final-state particles will be further filtered by imposing the energy-momentum conservation laws.

For the identification of the different final state particle we use the official CLAS12 Event-Builder [43]. In the following subsections we detail the main requirement for the different particles.

### 3.2.1 Electron Identification

For charged particles in the forward detectors, the Event Builder first assigns  $e^-$  (PID= 11) or  $e^+$  (PID= -11) (depending on the bending direction of the reconstructed track in the DC) if a particle satisfies all corresponding HTCC and ECAL requirements, and has an associated FTOF hit:

- 2.0 photoelectrons in HTCC.
- 60 MeV in PCAL.
- 5-sigma cuts on a parameterized momentum-dependent sampling fraction where "sampling fraction" is ECAL visible energy deposition (PCAL+Inner+Outer) divided by DC momentum.

In addition to these initial selections cuts, some regions of CLAS12 have to be excluded from the analysis to ensure an accurate detection of the different particles. For instance, an electron that hits the edge of the EC will have only part of its electromagnetic shower contained within the detector. Also, the structure of the torus magnet divides CLAS12 into six separate sectors, which makes edge effects non-negligible. Figure 3.1 shows the kinematic distributions of the DVCS electrons being detected and reconstructed in the forward detector of CLAS12 spectrometer in terms of the energy as a function of the polar angle ( $\theta$ ) and the azimuthal angle ( $\phi$ ) as a function of  $\theta$ .

### 3.2.2 Proton Identification

The slow recoiling final state protons will be detected within the BONuS12 RTPC. As the RTPC is physically within the CLAS12 simulation, but the track reconstruction is not finalized yet within CLAS12 reconstruction, we refer to a realistic fastmc that reproduces the expected performance of this detector. This fastmc has been developed initially from the BONuS6 experiment and tuned very precisely after EG6 experiment [44], which have used very similar RTPCs. This fastmc smears the proton's kinematics and applies acceptance

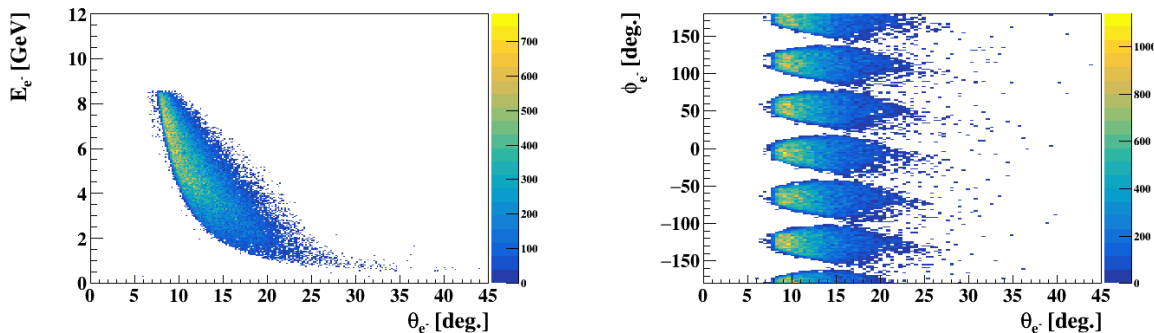


Figure 3.1: Electron’s energy as a function of it’s polar angle (left) and the azimuthal angle as a function of the polar angle (right), for n-DVCS events. Forward-CLAS12 acceptance and physics cuts are included.

functions. Regarding the smearing, the momentum, polar angle, azimuthal angle, and  $z$ -vertex of the protons are smeared with Gaussians using the observed tracking resolutions of the RTPC (see chapter 2, section 3 in [44]). For the acceptance, the fastmc:

- ensures that the proton’s track intersects with the cathode.
- removes the tracks which pass in the dead area between the two modules of the RTPC.
- rejects the track if it goes to the upstream end of the target’s holder.
- applies the RTPC’s thresholds on the momentum and the polar angle.

We do not specifically apply energy loss and multiple scattering in our fastmc, but we do apply resolution effects based on experimental data that include both effects. Figure 3.2 presents the kinematic distributions of the recoiling final state protons within the active volume of the BONUS12 RTPC.

### 3.2.3 Neutrals Identification

For neutrals, only photon (PID= 22) and neutron (PID= 2112) are considered, and particle identification is assigned based on simple beta cut at 0.9. Currently only one timing response is used for this, and for ECAL the prioritization is: PCAL, EC Inner, EC Outer. The momentum direction is assigned based on the neutral’s ECAL cluster position and the vertex of the charged particle used to determine the start time. For photons, the energy (magnitude of the momentum) is calculated from ECAL visible energy and momentum-dependent sampling fraction, while for neutrons energy is calculated from beta. For the central detector, CND is treated similarly as ECAL, except only neutron PID is assigned based on beta and the cut is at 0.8. Figure 3.3 presents the kinematic distributions of the neutron-DVCS photons being detected in the CLAS12 forward detector. Figure 3.4 shows

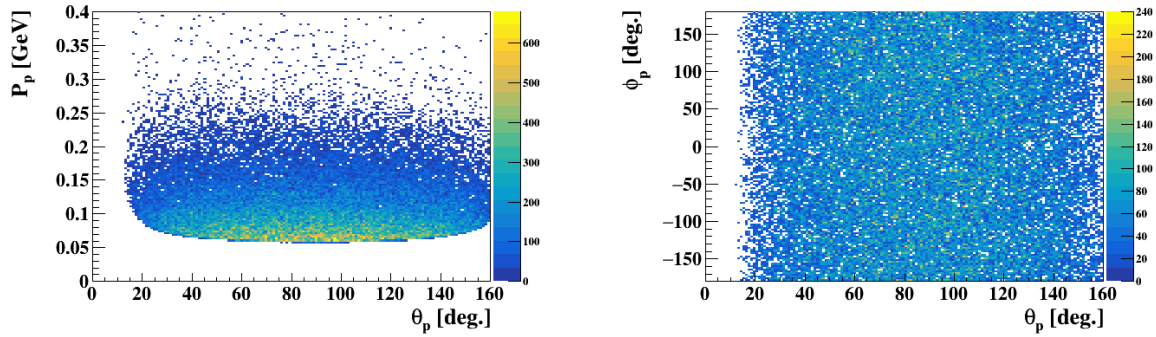


Figure 3.2: Recoiling proton’s momentum as a function of it’s polar angle (left) and the azimuthal angle as a function of the polar angle (right), from n-DVCS events. BONuS12 RTPC acceptance and physics cuts are included.

similar distributions of the detected final state neutrons being detected in both the forward and the central detectors of CLAS12 spectrometer. As can be seen from figures 3.1, 3.2, 3.3, 3.4, the DVCS electrons and photons are produced very forward, which is in a total agreement with our DVCS measurements during the 6 GeV era of CLAS, while slow recoiling protons are emitted more evenly in the polar angle range within the acceptance of the BONuS12 RTPC. The final neutrons are mostly emitted above  $\theta = 40^\circ$ , which is outside the acceptance of the forward detector of CLAS12 and was the main reason to upgrade CLAS12 with the Central neutron Detector during Run Group B to measure the neutron DVCS semi-exclusively (E12-11-003).

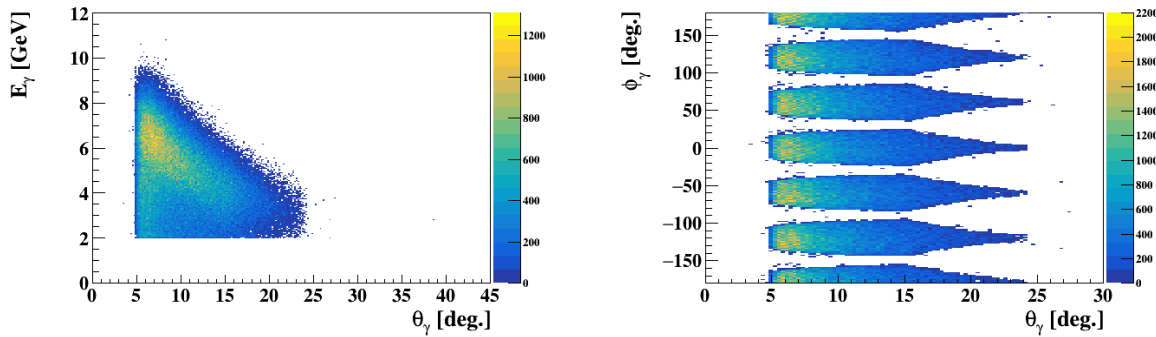


Figure 3.3: Photon’s energy as a function of it’s polar angle (left) and the azimuthal angle as a function of the polar angle (right), for n-DVCS events. Forward-CLAS12 acceptance and physics cuts are included.

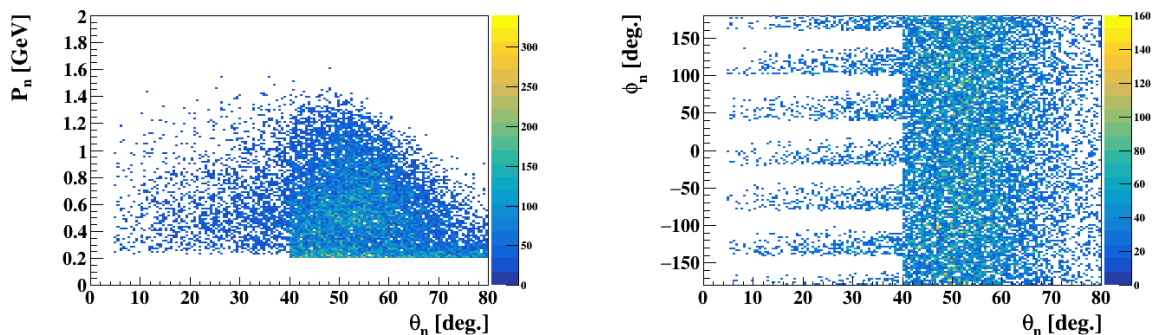


Figure 3.4: Recoiling neutron’s momentum as a function of it’s polar angle (left) and the azimuthal angle as a function of the polar angle (right), from n-DVCS events. BONuS12 forward and central acceptance and physics cuts are included.

### 3.3 Beam-Spin Asymmetry

The beam spin asymmetry of a longitudinally polarized electron beam on an unpolarized target ( $A_{LU}$ ) in each bin of the 108 total bins is defined as:

$$A_{LU} = \frac{1}{P_B} \frac{N^+ - N^-}{N^+ + N^-}. \quad (3.1)$$

where  $P_B$  is the beam polarization, and  $N^+$  and  $N^-$  are the number of events detected with positive and negative electron helicity, respectively. The statistical uncertainty of  $A_{LU}$  is

$$\sigma_{A_{LU}} = \frac{1}{P_B} \sqrt{\frac{1 - (P_B A_{LU})^2}{N}} \quad (3.2)$$

where  $N(= N^+ + N^-)$  is the total number of measured DVCS events in each bin.

It is particularly convenient to use the BSA  $A_{LU}$  as a DVCS observable, because most of the experimental systematic uncertainties, such as normalization and efficiencies that appear in the cross sections cancel out in the asymmetry ratio. However, some systematic uncertainties remain and they still contribute to the measured  $A_{LU}$ . The main known sources of systematic uncertainties are: the DVCS selection cuts, the fitting sensitivity to our binning, the beam polarization and the background (non exclusive  $\pi^0$ ) acceptance ratio. In the following, we present estimates of the contribution from each source based on our prior knowledge during CLAS-eg6 DVCS analysis [44].

In order to evaluate the systematic uncertainties stemming from the DVCS selection cuts, the eg6-analysis was repeated with changing the width of the exclusive cuts. The resulting systematic uncertainty to the  $A_{LU}$  asymmetry was around 6% for the incoherent DVCS channel. Because of the important improvement we expect with BONuS12 RTPC in terms of resolutions, we expect this uncertainty to be reduced to 4%.

Regarding the sensitivity of the fit results to our binning, the eg6 data were binned into two different bins in  $\phi$  and the reconstructed asymmetries were compared. The associated systematic uncertainty for  $A_{LU}$  at  $\phi = 90^\circ$  was found to be of 7.1%. For the proposed measurements, we expect to achieve higher statistics and therefore we reduced the expected systematics to 3%.

The beam polarization will be measured during the experiment by the Hall B Møller polarimeter. This polarimeter measures the angular distribution of the Møller electrons to obtain the beam polarization. The precision of the Hall B Møller polarimeter was measured to be around 3.5% [45]. We assume a 3.5% systematic uncertainty on the measured asymmetries similar to what was achieved during 6 GeV run.

A total systematic contributions is estimated to be around 11%. To be conservative, in particular because expected asymmetries on neutrons are much smaller than on protons, we used an increased total of 20% systematic uncertainty for our projections. This is added quadratically to the statistical error bars in each bin of the reconstructed asymmetry.

## 3.4 Projections

Once the final state particles being reconstructed and identified after passing all the physics and the geometry cuts. We reconstruct two types of neutron DVCS events as listed at the beginning of this chapter. Based on the approved Run Group F electron-nucleon running luminosity, a total of 9 million tagged and 850K fully exclusive neutron DVCS events will be collected during the 35 PAC days. In the following two subsections, we present our proposed binning for each set of data selection and the projections of the proposed measured beam-spin asymmetries.

### 3.4.1 Tagged n-DVCS Projections

After identifying the Tagged-neutron DVCS events, i.e., having only one electron, one photon, and one proton in the final state, we further filter them by imposing the energy-momentum conservation laws. Figure 3.5 shows the missing mass squared distribution of the identified tagged neutron DVCS events in addition to the missing energy distribution of these events. We apply an additional cut on the reconstructed missing mass squared to further clean the selected events as shown by the vertical red-dashed lines.

The spectator approximation assumes that the recoil proton is on its mass shell when the electron strikes the neutron and it gains neither energy nor momentum in during the interaction. In order to study the effect of Fermi motion on our measured DVCS observable, we specifically use the kinematics of the photons to determine the transferred momentum squared  $t$ . Figure 3.6 shows the distribution of  $Q^2$  as a function of  $x^*$  and  $x^*$  as a function of  $t$  of the identified tagged neutron DVCS events. On the right side plot of figure 3.6 we show the proposed binning in  $x^*$  versus  $-t$  space. The data will be binned three-dimensionally into 108 bins. That is, 12 bins in  $x^*$  vs.  $-t$ , and then nine bins in the azimuthal angle ( $\phi$ )

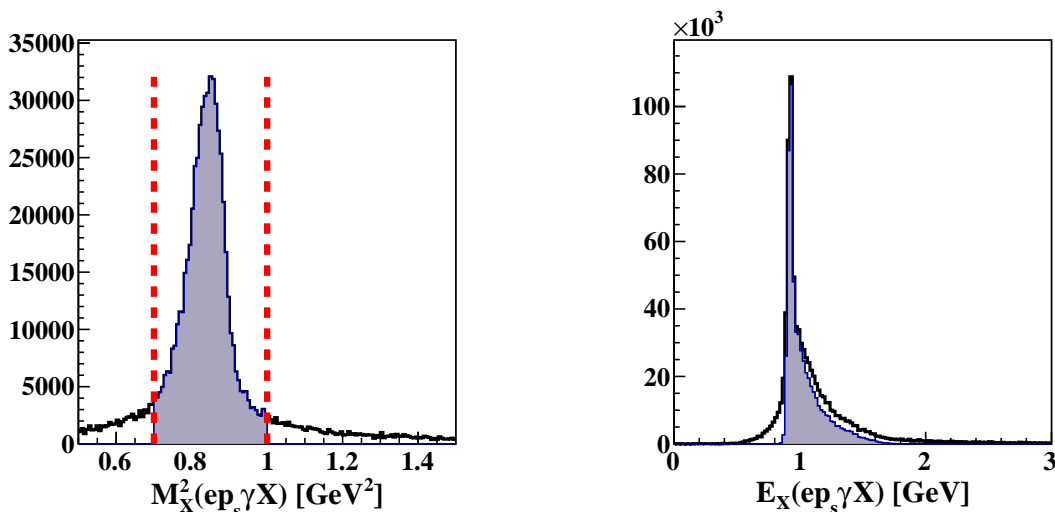


Figure 3.5: The distributions of the missing mass squared (left) and the missing energy (right) of the identified Tagged neutron DVCS events. The DVCS exclusivity cuts are represented by the vertical red-dashed lines. The black distributions represent the incoherent DVCS event candidates before the exclusivity cut. The shaded distributions represent the DVCS events that passed the cut on the missing mass squared.

for each of the 12 bins. The data are integrated over the full measured range of  $Q^2$ .

Figure 3.7 presents the reconstructed tagged neutron DVCS  $A_{LU}$  as a function of  $\phi$  in bins of  $x^*$  vs  $-t$ .

### 3.4.2 Fully exclusive n-DVCS projections

Our aim of this measurement is to investigate the Fermi motion and the final state interaction (FSI) effects on the measured neutron DVCS beam-spin asymmetry. This can be achieved by comparing the measured tagged neutron DVCS beam-spin asymmetry, that is by measuring  $d(e, e'p_s\gamma)X$ , to the measured full exclusive neutron DVCS channel, that is by measuring  $d(e, e'np_s\gamma)$ . The selection of the tagged DVCS events have been presented in the previous subsection, while different way of binning the data will be constructed as will be shown in this section.

Regarding the fully exclusive neutron DVCS events selection, events with the four final state particles being identified after applying all the geometry and physics cuts on the individual final state particle. After identifying these events, the exclusivity of the DVCS events is ensured by imposing a set of constraints based on the four-momentum conservation in the reaction  $ed \rightarrow e'p_s n\gamma$ . The distributions for the exclusive variables are shown in figure 3.8.

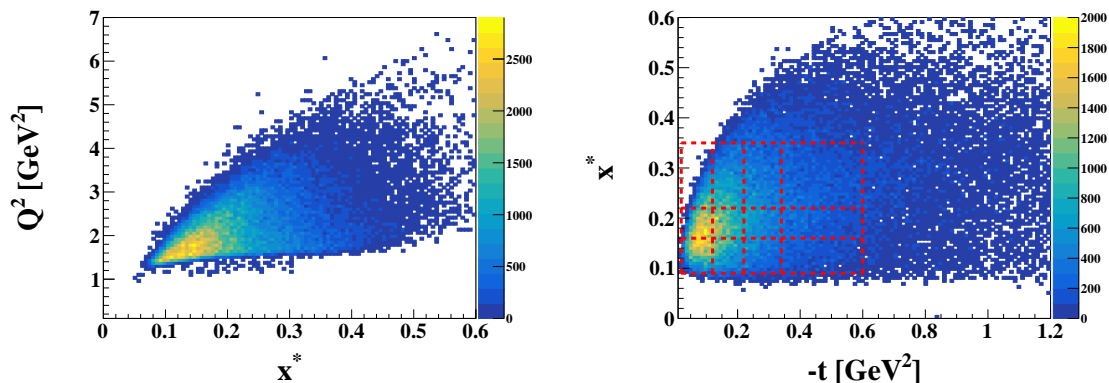


Figure 3.6: The distributions of the tagged neutron DVCS events in terms of  $Q^2$  versus  $x^*$  (left) and  $x^*$  versus  $-t$  (right). On the right we show the binning we proposed in  $x^*$  versus  $-t$  space.

As mentioned previously, a total of 850K fully exclusive events will be collected within the approved running luminosity and experimental setup of Run Group F. Similarly to the tagged DVCS events, we use the kinematics of the detected spectator proton to define the modified Lorentz invariant,  $x^*$ , and we define the transferred momentum squared,  $t$ , using the photons to investigate the initial Fermi motion effect on our DVCS observable of interest,  $A_{LU}$ . Figure 3.9 shows the distributions of  $Q^2$  as a function of  $x^*$  and  $x^*$  as a function of  $-t$  for the identified fully exclusive events. Before binning our data in the space of the momentum and the polar angle of the detected spectator momentum, we apply an initial cut on  $x^*$  vs.  $-t$ , as can be seen in Figure 3.9 which stands for the fully exclusive detected n-DVCS events. Similar cut is applied on the  $x^*$  vs.  $-t$  space of the tagged n-DVCS events. After that, both data sets are binned into 6 bins in the momentum of the spectator proton and its polar angle as shown in Figure 3.10. Finally, the data of each bin in  $p_s$  versus  $\theta_s$  is binned into 9  $\phi$  bins for the fully exclusive events and 12  $\phi$  bins for the tagged n-DVCS events. The reconstructed  $A_{LU}$  is presented in Figure 3.11 as a function of the hadronic angle  $\phi$  for the tagged n-DVCS events in black points and for the fully exclusive n-DVCS events in blue points. The error bars in these projections include both statistical and systematic uncertainties. We are considering 20% systematic uncertainties in our projections here as well. As one can see from our projections, the systematic uncertainties have the major contribution in the precision of our asymmetries and even with the extremely conservative assumption of 20% consideration, we will observe very precise beam-spin asymmetries.

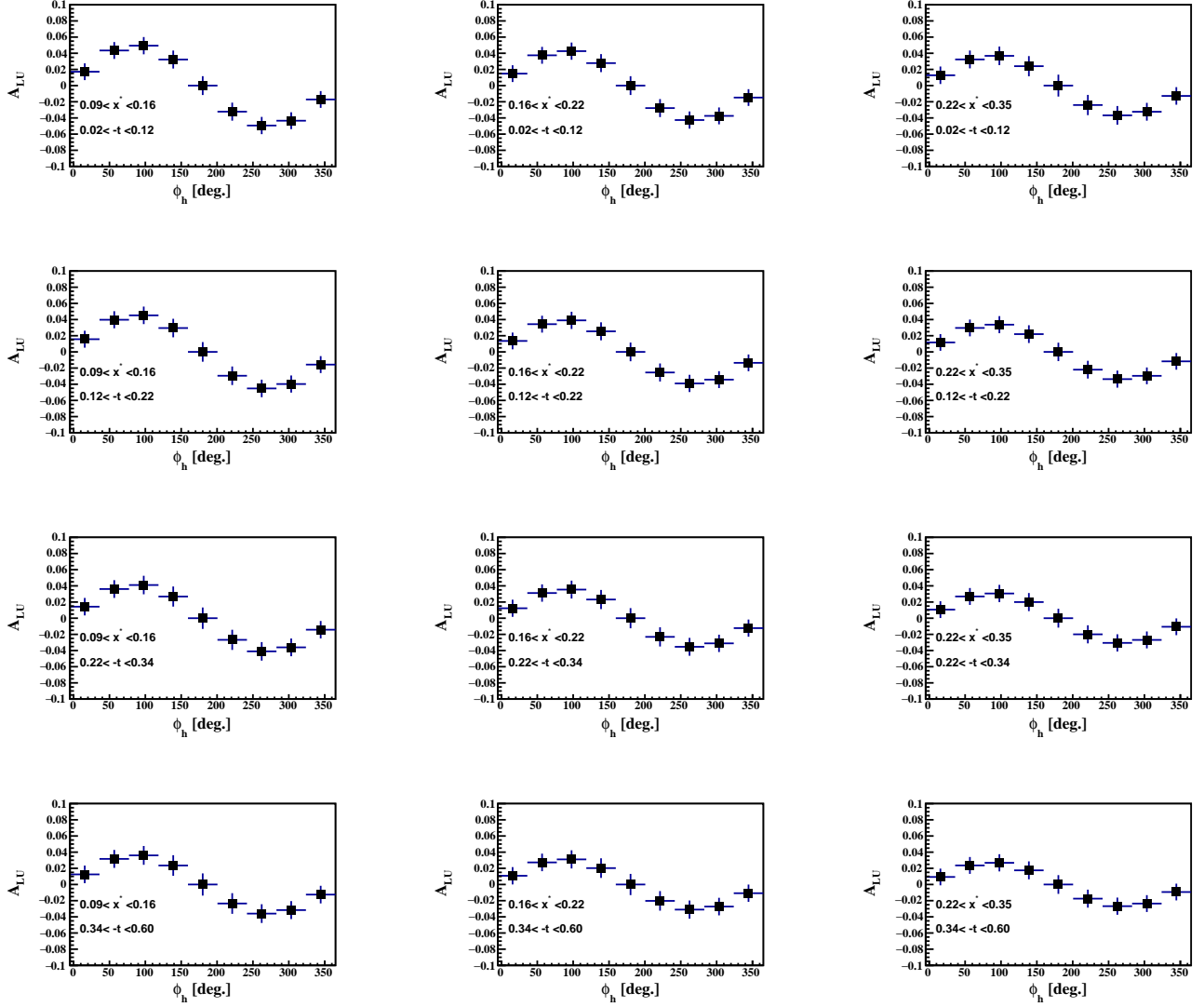


Figure 3.7: Projected beam-spin asymmetries as a function of the hadronic angle  $\phi_h$  in the binning of  $x^*$  vs  $-t$  space. The error bars include both the statistical and the systematic uncertainties added quadratically.

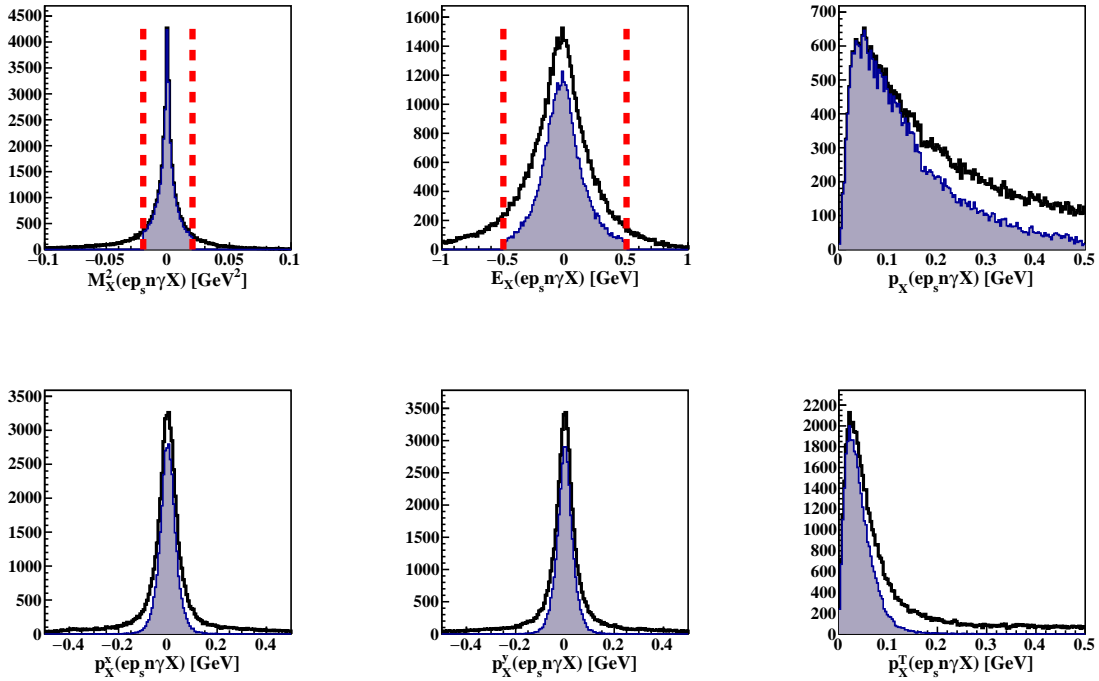


Figure 3.8: The distributions from left to right and from top to bottom are: missing mass squared, missing energy, missing total momentum, the x-component of the missing momentum, the y-component, and the transverse missing momentum in the  $e'p_s n \gamma$  final-state system. The DVCS exclusivity cuts are represented by the vertical red-dashed lines. The black distributions represent the DVCS event candidates before the exclusivity cuts. The shaded distributions represent the DVCS events that passed all of these cuts.

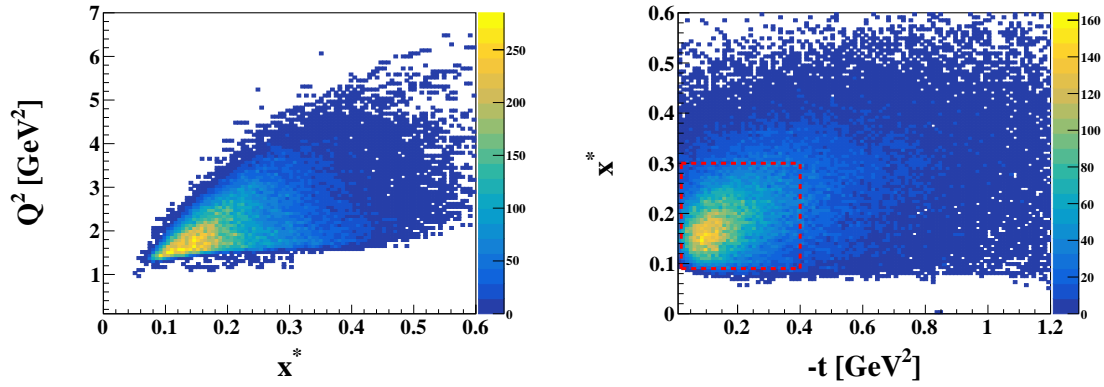


Figure 3.9: The distributions of the fully exclusive neutron DVCS events in terms of  $Q^2$  versus  $x^*$  (left) and  $x^*$  versus  $-t$  (right). On the right we show the bin of interest in  $x^*$  versus  $-t$  space.

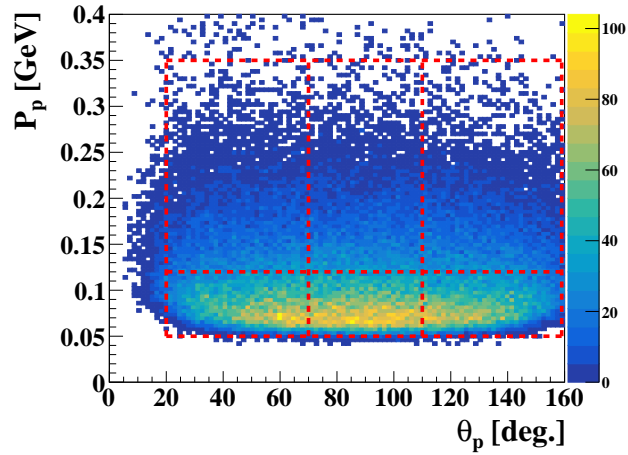


Figure 3.10: Data binning in  $p_s$  versus  $\theta_s$ .

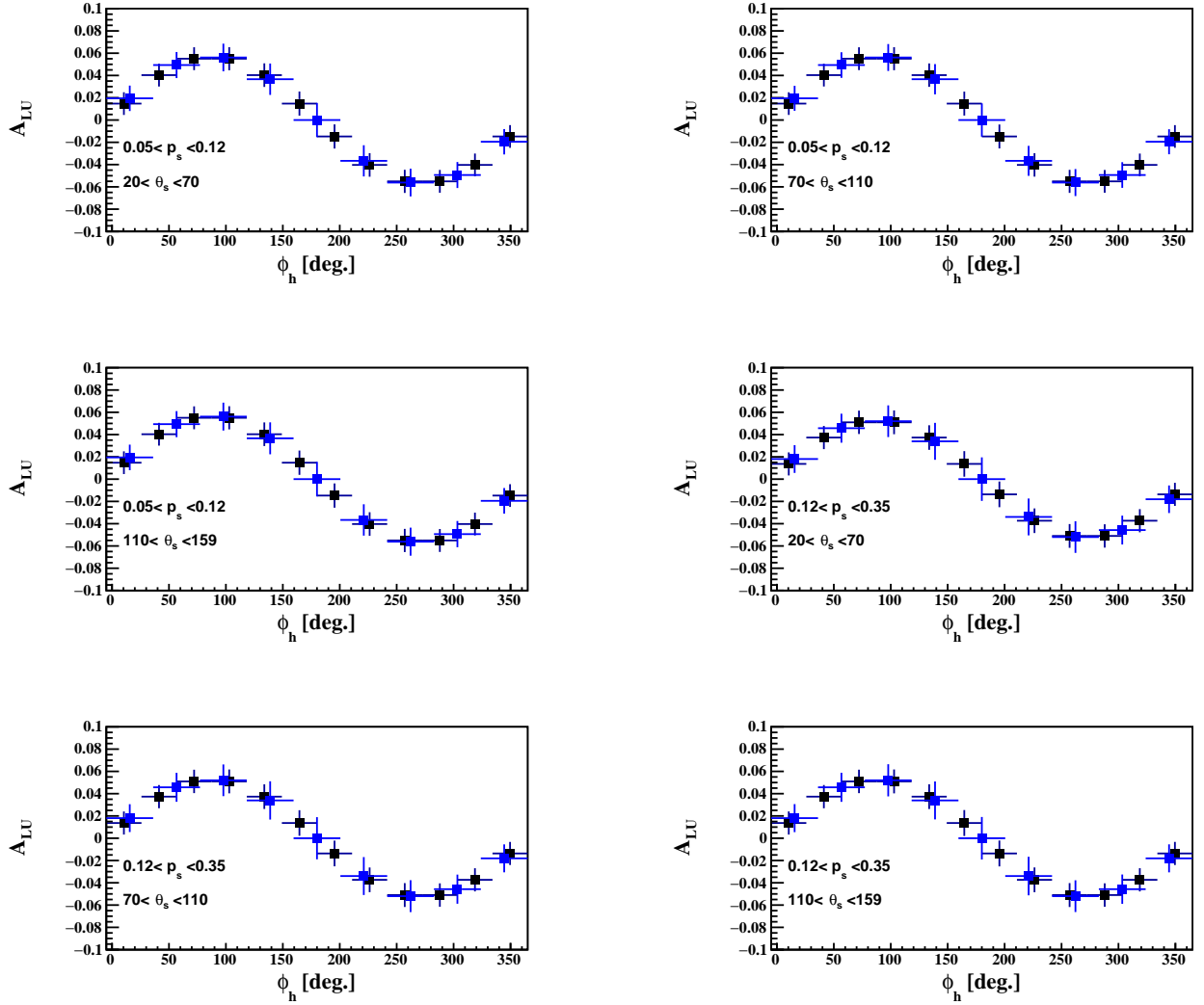


Figure 3.11: Projected beam-spin asymmetries as a function of the hadronic angle  $\phi_h$  in the binning of  $p_s$  vs  $\theta_s$  space. The error bars include both the statistical and the systematic uncertainties added quadratically.

# Chapter 4

## Additional Physics Measurements with Run Group F

The combination of the high luminosity available at Jefferson Lab, the large acceptance of CLAS12 detector and the BONuS12 RTPC offers an amazing opportunity to advance our understanding of long standing mysteries in QCD. This new development in detection capabilities, will allow the study of medium modification with a handle on Fermi motion uncertainties and FSI effects. It is therefore clear that the focus of the neutron DVCS proposal is only a fraction of the physics that can be achieved by successfully analyzing the Run Group F data with highly polarized beam. This data will be a gold mine, which will allow us to investigate in a unique way several important physics questions and conquer new territories in the nuclear QCD land. Some of the topics of interest to increase the physics outcome of BONuS12 polarized beam data are:

- Coherent DVCS and deeply virtual mesons production (DVMP) off deuteron. For DVMP, we can study for example  $\pi^0$ ,  $\phi$ ,  $\omega$  and  $\rho$  mesons.
- Incoherent proton DVCS and DVMP off bound deuterium.
- Deep virtual  $\pi^0$  production off neutron, which is interesting by itself but also the background of DVCS measurements.
- Semi-inclusive reaction  $p(e,e'p)X$  to study the  $\pi^0$  cloud of the proton and  $D(e,e'pp_S)X$  to study the  $\pi^-$  cloud of the neutron, at very low proton momenta.
- The medium modification of the transverse momentum dependent parton distributions.

# Summary

In summary, polarizing the electron beam during the approved E12-06-113 experiment (BONuS12) will allow us to investigate in a unique way many aspects of QCD within the GPD framework. The approved E12-11-003 experiment, “Deeply Virtual Compton Scattering on the Neutron with CLAS12 at 11 GeV” is set to measure the n-DVCS beam-spin asymmetry by directly detecting the struck neutron in the reaction  $\gamma^* + d \rightarrow n + \gamma + (p)$ . While we intend to measure the neutron DVCS beam-spin asymmetry by tagging the spectator slow-recoiling proton in addition to measuring the fully exclusive neutron DVCS channel. The first channel will enrich our knowledge about the partonic structure of the quasi-free neutrons, while the fully exclusive neutron DVCS measurement will be a golden data set to understand the Fermi motion and final state interaction effects on the measured DVCS beam-spin asymmetries. While this proposal is focusing only on the neutron DVCS measurements, highly polarizing the beam during Run Group F will be giving us a golden chance to measure additional physics topics, increasing the physics outcome of the approved beam time and advancing our understanding on many aspects of QCD.

# Bibliography

- [1] M. Burkardt, “Impact parameter dependent parton distributions and off-forward parton distributions,” *Phys. Rev.*, vol. D62, p. 071503, 2000.
- [2] M. Diehl, “Generalized parton distributions in impact parameter space,” *Eur.Phys.J.*, vol. C25, pp. 223–232, 2002.
- [3] A. V. Belitsky and D. Mueller, “Nucleon hologram with exclusive lepton production,” *Nucl. Phys.*, vol. A711, pp. 118–126, 2002.
- [4] M. Burkardt, “Transverse deformation of parton distributions and transversity decomposition of angular momentum,” *Phys. Rev.*, vol. D72, p. 094020, 2005.
- [5] X.-D. Ji, “Gauge-Invariant Decomposition of Nucleon Spin,” *Phys. Rev. Lett.*, vol. 78, pp. 610–613, 1997.
- [6] E. Leader and C. Lorcé, “The angular momentum controversy: What’s it all about and does it matter?,” *Phys. Rept.*, vol. 541, no. 3, pp. 163–248, 2014.
- [7] M. Hattawy *et al.*, “Deeply Virtual Compton Scattering measurement off bound protons,” 2018.
- [8] M. Amaryan *et al.*, “The Structure of the Free Neutron at Large x-Bjorken (E12-06-113),” *A proposal to PAC 30*, 2006.
- [9] D. Müller, D. Robaschik, B. Geyer, F. M. Dittes, and J. Horejsi, “Wave functions, evolution equations and evolution kernels from light ray operators of QCD,” *Fortsch. Phys.*, vol. 42, pp. 101–141, 1994.
- [10] X. Ji, “Deeply virtual compton scattering,” *Phys. Rev. D*, vol. 55, pp. 7114–7125, Jun 1997.
- [11] A. V. Radyushkin, “Scaling limit of deeply virtual Compton scattering,” *Phys. Lett.*, vol. B380, pp. 417–425, 1996.
- [12] A. V. Radyushkin, “Nonforward parton distributions,” *Phys. Rev. D*, vol. 56, pp. 5524–5557, Nov 1997.

- 
- [13] S. Stepanyan *et al.*, “Observation of exclusive deeply virtual compton scattering in polarized electron beam asymmetry measurements,” *Phys. Rev. Lett.*, vol. 87, p. 182002, Oct 2001.
- [14] A. Airapetian *et al.*, “Measurement of the beam-spin azimuthal asymmetry associated with deeply-virtual compton scattering,” *Phys. Rev. Lett.*, vol. 87, p. 182001, Oct 2001.
- [15] A. Airapetian *et al.*, “Beam-charge azimuthal asymmetry and deeply virtual compton scattering,” *Phys. Rev. D*, vol. 75, p. 011103, Jan 2007.
- [16] F. X. Girod *et al.*, “Measurement of Deeply virtual Compton scattering beam-spin asymmetries,” *Phys. Rev. Lett.*, vol. 100, p. 162002, 2008.
- [17] M. Defurne *et al.*, “E00-110 experiment at jefferson lab hall a: Deeply virtual compton scattering off the proton at 6 gev,” *Phys. Rev. C*, vol. 92, p. 055202, Nov 2015.
- [18] M. Mazouz *et al.*, “Deeply virtual compton scattering off the neutron,” *Phys. Rev. Lett.*, vol. 99, p. 242501, Dec 2007.
- [19] G. Gavalian *et al.*, “Beam spin asymmetries in deeply virtual compton scattering (dvcs) with clas at 4.8 gev,” *Phys. Rev. C*, vol. 80, p. 035206, Sep 2009.
- [20] E. Seder *et al.*, “Longitudinal target-spin asymmetries for deeply virtual compton scattering,” *Phys. Rev. Lett.*, vol. 114, p. 032001, Jan 2015.
- [21] H. S. Jo *et al.*, “Cross sections for the exclusive photon electroproduction on the proton and Generalized Parton Distributions,” *Phys. Rev. Lett.*, vol. 115, no. 21, p. 212003, 2015.
- [22] M. Guidal, H. Moutarde, and M. Vanderhaeghen, “Generalized Parton Distributions in the valence region from Deeply Virtual Compton Scattering,” *Rept. Prog. Phys.*, vol. 76, p. 066202, 2013.
- [23] R. Dupré, M. Guidal, and M. Vanderhaeghen, “Tomographic image of the proton,” *Phys. Rev. D*, vol. 95, p. 011501, Jan 2017.
- [24] R. D. Ball *et al.*, “Parton distributions for the LHC Run II,” *JHEP*, vol. 04, p. 040, 2015.
- [25] M. Mazouz *et al.*, “Deeply virtual compton scattering off the neutron,” *Phys. Rev. Lett.*, vol. 99, p. 242501, 2007.
- [26] N. d’Hose, S. Niccolai, and A. Rostomyan, “Experimental overview of Deeply Virtual Compton Scattering,” *Eur. Phys. J.*, vol. A52, no. 6, p. 151, 2016.

- [27] R. Dupré, M. Guidal, S. Niccolai, and M. Vanderhaeghen, “Analysis of Deeply Virtual Compton Scattering Data at Jefferson Lab and Proton Tomography,” *Eur. Phys. J.*, vol. A53, no. 8, p. 171, 2017.
- [28] H. Moutarde, P. Sznajder, and J. Wagner, “Border and skewness functions from a leading order fit to DVCS data,” *Eur. Phys. J.*, vol. C78, no. 11, p. 890, 2018.
- [29] K. Goeke, M. V. Polyakov, and M. Vanderhaeghen, “Hard exclusive reactions and the structure of hadrons,” *Prog. Part. Nucl. Phys.*, vol. 47, pp. 401–515, 2001.
- [30] M. Diehl, “Generalized parton distributions with helicity flip,” *Eur. Phys. J.*, vol. C19, pp. 485–492, 2001.
- [31] A. V. Belitsky, D. Mueller, and A. Kirchner, “Theory of deeply virtual Compton scattering on the nucleon,” *Nucl. Phys.*, vol. B629, pp. 323–392, 2002.
- [32] A. V. Belitsky, D. Mueller, L. Niedermeier, and A. Schafer, “Leading twist asymmetries in deeply virtual Compton scattering,” *Nucl. Phys.*, vol. B593, pp. 289–310, 2001.
- [33] C. Ciofi degli Atti, L. P. Kaptari, and B. Z. Kopeliovich, “Final state interaction effects in semiinclusive DIS off the deuteron,” *Eur. Phys. J.*, vol. A19, pp. 145–151, 2004.
- [34] C. Ciofi degli Atti and B. Z. Kopeliovich, “Final state interaction in semiinclusive DIS off nuclei,” *Eur. Phys. J.*, vol. A17, pp. 133–144, 2003.
- [35] “CLAS12 Technical Design Report,” 2008.
- [36] S. Kuhn , *Private communication*.
- [37] A. E. Alaoui and E. Voutier *CLAS Note 2009-024*.
- [38] M. Vanderhaeghen, P. A. M. Guichon, and M. Guidal, “Deeply virtual electroproduction of photons and mesons on the nucleon: Leading order amplitudes and power corrections,” *Phys. Rev. D*, vol. 60, p. 094017, Oct 1999.
- [39] M. Guidal, M. V. Polyakov, A. V. Radyushkin, and M. Vanderhaeghen, “Nucleon formfactors from generalized parton distributions,” *Phys. Rev.*, vol. D72, p. 054013, 2005.
- [40] M. Lacombe, B. Loiseau, J. M. Richard, R. V. Mau, J. Côté, P. Pirès, and R. de Tournell, “Parametrization of the paris  $n - n$  potential,” *Phys. Rev. C*, vol. 21, pp. 861–873, Mar 1980.
- [41] *CLAS12 GEMC simulation*, <https://gemc.jlab.org/gemc/html/index.html>.
- [42] *CLAS12 CLARA*, <https://claraweb.jlab.org/claraweb/>.
- [43] *CLAS12 Event-Builder*, [https://clasweb.jlab.org/wiki/index.php/CLAS12\\_EventBuilder#Particle\\_Identification](https://clasweb.jlab.org/wiki/index.php/CLAS12_EventBuilder#Particle_Identification).

- 
- [44] M. Hattawy *and others* (EG6 Working Group), “Deeply Virtual Compton Scattering off  $^4\text{He}$ ,” *CLAS internal analysis note*, 2016.
- [45] J. M. Grames *et al.*, “Unique electron polarimeter analyzing power comparison and precision spin-based energy measurement,” *Phys. Rev. ST Accel. Beams*, vol. 7, p. 042802, Apr 2004.